Available online at www.sciencedirect.com
ScienceDirect
Journal of Magnetic Resonance 186 (2007) 305–310
JMR Journal of Magnetic Resonance
www.elsevier.com/locate/jmr

Simultaneous acquisition of magnetic resonance spectroscopy (MRS) data and positron emission tomography (PET) images with a prototype MR-compatible, small animal PET imager

Raymond R. Raylman [a,*], Stan Majewski [b], S. Sendhil Velan [a], Susan Lemieux [a], Brian Kross [b], Vladimir Popov [b], Mark F. Smith [b], Andrew G. Weisenberger [b]

[a] *Center for Advanced Imaging, Department of Radiology, West Virginia University, HSCS Box 9236, Morgantown, WV 26506, USA*
[b] *Detector and Imaging Group, Thomas Jefferson National Accelerator Facility, Newport News, VA, USA*

Received 14 August 2006; revised 1 March 2007
Available online 24 March 2007

Abstract

Multi-modality imaging (such as PET–CT) is rapidly becoming a valuable tool in the diagnosis of disease and in the development of new drugs. Functional images produced with PET, fused with anatomical images created by MRI, allow the correlation of form with function. Perhaps more exciting than the combination of anatomical MRI with PET, is the melding of PET with MR spectroscopy (MRS). Thus, two aspects of physiology could be combined in novel ways to produce new insights into the physiology of normal and pathological processes. Our team is developing a system to acquire MRI images and MRS spectra, and PET images contemporaneously. The prototype MR-compatible PET system consists of two opposed detector heads (appropriate in size for small animal imaging), operating in coincidence mode with an active field-of-view of ~14 cm in diameter. Each detector consists of an array of LSO detector elements coupled through a 2-m long fiber optic light guide to a single position-sensitive photomultiplier tube. The use of light guides allows these magnetic field-sensitive elements of the PET imager to be positioned outside the strong magnetic field of our 3T MRI scanner. The PET scanner imager was integrated with a 12-cm diameter, 12-leg custom, birdcage coil. Simultaneous MRS spectra and PET images were successfully acquired from a multi-modality phantom consisting of a sphere filled with 17 brain relevant substances and a positron-emitting radionuclide. There were no significant changes in MRI or PET scanner performance when both were present in the MRI magnet bore. This successful initial test demonstrates the potential for using such a multi-modality to obtain complementary MRS and PET data.

Keywords: Positron emission tomography; Magnetic resonance spectroscopy; Multi-modality imaging

1. Introduction

The complementary information obtainable with positron emission tomography (PET) imagers and magnetic resonance imaging (MRI) scanners can potentially improve the detection and diagnosis of a number of disease states. Specifically, the ability to correlate physiology (PET images) with morphology (MRI images) facilitates the accurate identification and positioning of abnormal tissues. The utility of combining morphology and physiology in clinical and research applications has been demonstrated by the use of PET–CT scanners. What is perhaps more exciting is the ability to combine PET images with magnetic resonance spectroscopy (MRS) data. Correlation of these data could prove to be an extremely powerful research and diagnostic tool. For example, PET images could be applied to the identification of metabolically active areas of a tumor to be targeted by MRS. Furthermore, the inherently spatially and temporally co-registered MRS–PET images could greatly facilitate correlation of

* Corresponding author. Fax: +1 304 293 4287.
E-mail address: rraylman@wvu.edu (R.R. Raylman).

1090-7807/$ - see front matter © 2007 Elsevier Inc. All rights reserved.
doi:10.1016/j.jmr.2007.03.012

metabolite distributions with images of metabolic activity or neuro-receptor densities acquired with PET. In addition, quantitative measurements of physiologic parameters obtained with PET (such as perfusion or glucose metabolism) could be integrated with metabolite profiles obtained with MRS to provide additional insights into a number of disease processes. The combination of PET-derived metabolic information (perhaps even quantitative results from the kinetic modeling of dynamic data), with metabolite profiles or metabolite imaging with spatial–spectral sequences (MRSI) could allow for unique applications of this new technology. Finally, the contemporaneous acquisition of MRS data and PET images could also significantly reduce the complications (changes in scanner performance or patient physiology) inherent in correlating functional images acquired with separate scanners at different times.

While there are significant advantages to creation of a combined MRI–PET scanner, there are also some significant obstacles to this integration. The strong static magnetic fields required for MRI and MRS significantly degrade the performance of standard photomultiplier tubes (PMT) used in most PET scanners to convert light produced in the scintillator to amplified electrical signals. Specifically, the magnetic component of the Lorentz force deflects the accelerating electrons in PMTs, producing significant degradation of their performance. In addition, electrical noise produced by components of PET detectors (such as the PMTs) may induce significant artifacts in MRI images.

One approach to solving this problem is to replace the PMTs with avalanche photodiodes (APD) [1–3]. APDs are solid-state devices that have moderate gain, but are virtually unaffected by strong magnetic fields. For example, a group at the University of Tübingen has created an MRI-compatible PET scanner insert based on APDs [4]. They found that to prevent damaging these devices it was necessary to shield the APDs from the strong gradient magnetic fields present during many MRI pulse sequences. The presence of this shielding, however, was found to reduce MRI signal-to-noise ratios (SNR) by approximately 20% in gradient echo (GRE) and spin–echo (SE) images. Another group is investigating the use of short light guides to transport light from the scintillator to arrays of APDs located just outside of the MRI imaging area, thus eliminating the need for APD shielding and the resulting loss of SNR [5].

Our group's approach is to continue the use of PMTs, since they have some very desirable characteristics (high gain and proven reliability), removing them from the main static and gradient magnetic fields of the MRI scanner. Thus, the Lorentz force's effect on the PMTs is reduced. Specifically, fiber optic light guides are used to transmit light from scintillator arrays to PMTs located outside the bore of the magnet. This approach has been previously utilized with some success [6–8]. For example, Garlick et al. have demonstrated the potential of this capability by constructing a combined NMR–PET system using light guides and PMTs to simultaneously acquire ^{31}P spectra and ^{18}F-fluorodeoxyglucose (FDG) uptake maps (acquired with a PET system) of an isolated rat heart in a 9.4 T NMR system [9,10]. While initial simultaneous MRI and PET images have been obtained by a number of groups, and MRS spectra have been acquired from specialized high-filed NMR systems in concert with PET imaging, very little work has been performed demonstrating the acquisition of spectroscopic data (1D and 2D correlated spectra) and PET images on a larger bore MRI scanner. Thus, the goal of our initial investigation was to determine the feasibility of simultaneously acquisition of MRS and PET data using a fiber optically coupled PET imager using a wide-bore 3T MRI scanner.

2. Experimental

2.1. MRI–PET scanner

The two prototype MRI-compatible PET detector modules consisted of 20×20 arrays of $2.5 \times 2.5 \times 15\ mm^3$ lutetium oxyorthosilicate (LSO) scintillator detector elements (2.6 mm center-to-center separation). These arrays were connected to the photodetectors [flat panel position-sensitive photomultiplier tubes (PSPMTs)] via 2.5 m long fiber optic light guides (cross-section $5 \times 5\ cm^2$) made up of glued arrays of 2 mm diameter fiber optic cables (Mitsubishi Optical Corp.). The light guides were bent by 90° at their input ends to allow the scintillator arrays (to which they were coupled) to face objects in the MRI scanner's bore. In addition to reducing the physical size of the PET detectors, the use of flat panel PSPMTs (Hamamatsu Inc. Model H8500) is desirable because the performance of these devices is not severely degraded by the presence of the magnetic field ($\sim$200 G oriented at an angle of $\sim$20° with the front face of the PMTs) outside the bore of the MRI magnet, due to their relatively short dynode chain. To further reduce the effects of the magnetic field at the location of the PSPMTs, a 1.3-mm thick sheet of magnetic shielding foil (Magnetic Shield Corp.) was applied to the outside of each unit. The PSPMTs were read out using resitive-strip circuitry. X and Y outputs from the readouts were amplified with custom amplifier boards prior to processing by two analog-to-digital converters (ADC, LeCroy FERA 4300B). The last dynodes of both PSPMTs were used to provide a common 300 ns-wide coincidence trigger pulse to the ADCs [11]. A 6-ns coincidence window was applied to reduce acceptance of random coincidence events. No attenuation correction measurements were made in this current system. It is important to note that the PET device described in this work is a demonstration prototype intended to explore the feasibility of performing MRI and MRS measurements simultaneously with acquisition of PET images. The optimize design of the scanner will consist of a complete ring of detector heads, allowing the creation of true tomographic images.

Data acquisition was controlled with software written using the Kmax programming environment (Sparrow, Inc.) resident on a G4 Apple Macintosh® Power PC. Since our prototype PET scanner had just two detector arrays, it sampled only a limited portion of the emitted photons. These two MRI–PET modules (LSO array, light guide and PSPMT) were mounted in an acrylic frame. The separation between the two detectors was 14 cm. Hence, the imager has a field-of-view of $5 \times 5 \times 14$ cm^3 and a spatial resolution of ~2.6 mm. Light loss in the light guides reduced the energy resolution of the PET system is ~85%. Additional details of the construction and performance PET component of our MRI–PET imager are given elsewhere [12]. A 12-cm diameter, 12-leg birdcage coil was integrated with the PET scanner to produce our prototype system. This coil, manufactured by Nova Medical, Inc., operates in the transmit/receive mode tuned at 127.7 MHz for use in a 3T General Electric Medical Systems Inc., Signa long-bore scanner.

2.2. Multi-modality spectroscopy phantom

To assess the ability to simultaneously acquire PET and MRI, and PET and MRS data a spherical, multi-modality phantom was constructed. Specifically, a 30-mm diameter hollow glass sphere was filled with 17 substances commonly found in the human brain. The concentrations of each chemical in the phantom were [13]: GABA 1 mM, L-aspartate (Asp) 1 mM, choline (Ch) 0.9 mM, creatine (Cr) 5.4 mM, ethanolamine (Et) 3.3 mM, glucose (Glc) 1 mM, glutamate (Glu) 8.1 mM, glutamine (Gln) 1.6 mM, glutathione (GSH) 2 mM, glycerophosphorylcholine (GPC) 1 mM, myo-inositol (mI) 3.5 mM, lactate (Lac) 0.4 mM, phosphocreatine (PC) 1.6 mM, phosphorylcholine (PCh) 0.6 mM, taurine (Tau) 0.9 mM, *N*-acetyl aspartate (NAA) 7.6 mM and threonine (Thr) 0.3 mM. The metabolites were prepared in a buffer containing 1 mM DSS, 72 mM K_2HPO_4, 28 mM KH_2PO_4, 200 mM Na formate, 1 g/l NaN_3. The pH of the mixture was adjusted to be 7.2. To produce the PET signal, 0.12 μCi/ml of ^{18}F-fluorodeoxyglucose (a commonly used positron-emitting radiopharmaceutical) was added to the sphere (total radioactivity was ~14.4 μCi) approximately 5 min prior to data acquisition. Fig. 1 shows the phantom inside the MRI–PET imaging insert.

2.3. MRI and MRS phantom data acquisition

All experiments were performed using a General Electric 3T MRI/MRS scanner running on the Excite platform equipped with self-shielded gradients (40 mT/m). Gradient-echo images were acquired using a 3D spoiled gradient echo pulse-sequence (SPGR) with 1-mm-thick slices and in-plane spatial resolution of 312×312 μm, repetition time (TR) of 9.5 ms, 15° flip angle two excitations (NEX) and an echo time (TE) of 2.2 ms. Spin–echo images were acquired with a fast spin–echo sequence with 3.2 mm thick slices and in-plane spatial resolution of 312×312 μm, TR of 2.525 s, NEX of 2 with an echo train length of 8 and a minimum echo time of 14.1 ms.

The gradient echo images were used to target the volume of interest (VOI) for MRS measurements. All spectroscopic data acquisitions used a $1.5 \times 1.5 \times 1.5$-cm^3 (3.375 ml) target volume. Manual shimming was performed to reduce magnetic field inhomogeniety. Localized one-dimensional MR spectral data were recorded using a PRESS sequence [14] consisting of three-selective RF pulses (90°–180°–180°) employing the Shinnar–LeRoux algorithm [15]. The 90° pulse was transmitted for 3.6 ms at a bandwidth of 2.4 kHz and the 180° pulse bandwidth was 1.4 kHz for duration of 5.2 ms. The second-half of the 2nd spin–echo was acquired from protons located at the intersection of the three slices in the VOI. An echo time of 30 ms and a repetition time of 2 s were employed for 128 averages.

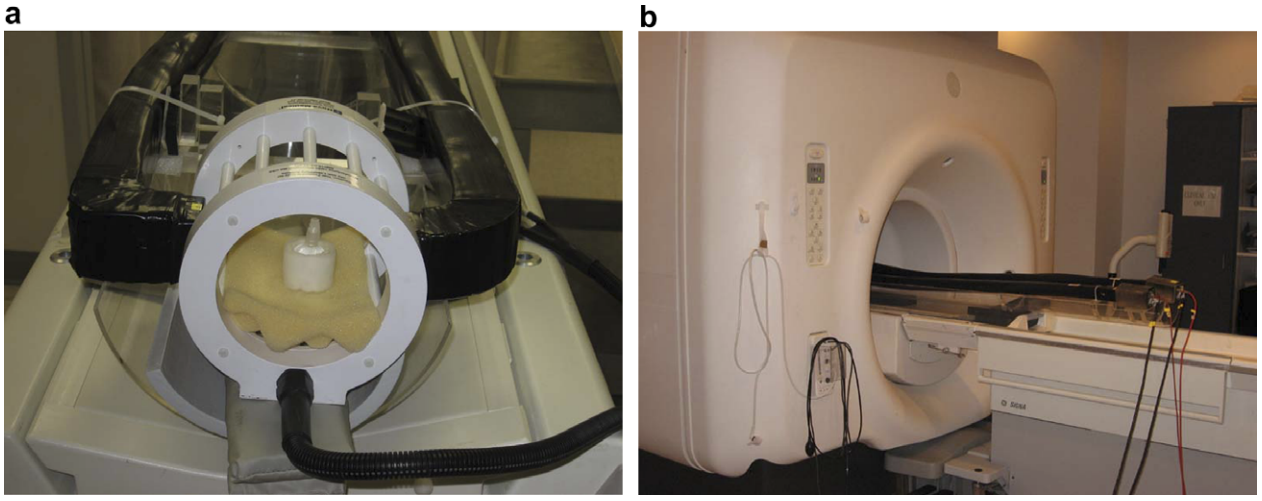

Fig. 1. Pictures showing the MRI–PET imaging insert. (a) The multi-modality spectroscopy phantom in MRI–PET imaging insert and (b) the insert at its scanning position in the 3T MRI scanner.

Use of a short, 30-ms long echo time minimizes J modulation and reduces signal losses due to T_2 relaxation [16]. All measurements were performed with 2048 complex points for acquisition and a spectral width of 5 kHz. Unsuppressed water spectra from the VOI were acquired with 16 averages for all data acquisitions. The 1D MRS spectra were quantified with LC Model software [17].

In addition to the 1D spectra, a localized, two-dimensional correlated spectroscopy (L-COSY) sequence [18] employing two echoes, a spin–echo and a coherence transfer echo, was used to record the 2D MRS data following the 1D MRS measurements. The CHESS water suppression module and outer volume saturation module (General Electric Medical Systems Inc.) were identical to those employed with the 1D PRESS sequence described above. The L-COSY sequence was designed using similar RF pulses as employed for the PRESS pulse sequence [19,20]. The same VOI used for the 1D MRS experiments was localized in one shot by a combination of three slice selective RF pulses (90°–180°–90°) in combination with appropriate B_0 crusher gradient pulses. The last 90° RF pulse facilitates both slice selection and coherence transfer. An incremental period for the second dimension was inserted immediately after the formation of spin–echo. B_0 crusher gradients were applied around the second 180° and the third 90° pulses. The duration was 30 ms, with an incremental period of 0.8 ms, resulting in a spectral bandwidth of 1.25 kHz. Sixty-four t_1 increments were performed for all 2D measurements. Each incremental period was averaged over 32 scans. The second-half of the coherence transfer echo was sampled using 2048 complex points. The post processing of all 2D data sets were performed using FELIX software (Accelrys Inc, San Diego, CA). The spectral bandwidth was set to 5000 Hz along the acquisition dimension (t_2) described by 2048 complex points and to 1250 Hz along the indirectly detected t_1 dimension. Note that both MRI and MRS data were acquired with the PET imaging component present and absent from the MRI scanner's bore to assess the potential effects of the device on the results. Signal-to-noise ratios (SNR) were measured on the SPGR and FSE MRI images by calculating the mean pixel intensity from a 15-mm diameter region-of-interest (ROI) in the center of the image of the sphere. Noise was estimated by calculating the standard deviation of the same sized ROI positioned at five locations outside the image of the sphere. Thus, five SNRs were determined, from which a mean and standard deviation were calculated for each scanning condition and pulse sequence. Additionally, NAA/Cr ratios were calculated from the 1D and L-COSY spectra. This ratio is often used in the clinical evaluation of tumors.

2.4. PET phantom data acquisition and reconstruction

PET data acquisition was performed during the execution of the MRI and MRS pulse sequences described above. List mode data were acquired for 10 min; the average true count rate was approximately 2000 events/s. Because this prototype device does not fully sample the 180° necessary for optimal image reconstruction, the PET images were reconstructed with a limited angle, maximum likelihood expectation maximization (MLEM) algorithm [11] ($2 \times 2 \times 2$ mm^3 reconstructed voxels). Since limited angle tomography was used, images in the planes perpendicular to the scanner axis (the transaxial planes) were subject to blurring caused by angular under-sampling. Therefore, we utilized the sagittal views (plane parallel to the axis of the scanner) of the object. At this early stage in development of our system, the MRI and PET images were aligned manually using standard image display software. A more sophisticated automated co-registration software package is currently under development.

3. Results

Fig. 2 shows the results from the PET and MRI imaging procedures. Specifically, the PET, SPGR MRI images and co-registered SPGR and PET images are shown. There were no unusual PET image artifacts caused by the presence of the strong main magnetic field, gradient magnetic fields or RF. The PET image is non-optimal due to the limited angle nature of the data acquired with this prototype system. The SNRs measured from the SPGR images were 26.7 ± 1.9 and 26.8 ± 0.8 with and without PET imager in the MRI scanner, respectively. Similar measurements using the FSE images yielded SNRs of 302.5 ± 7.4 and 298.7 ± 9.1 with and without PET scanner present,

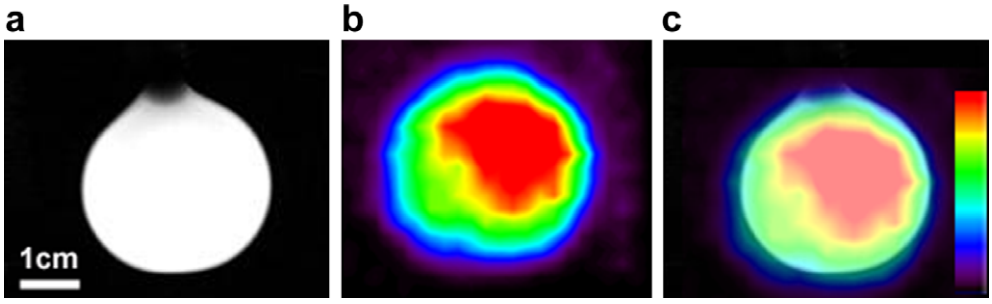

Fig. 2. Images from the MRI–PET system. (a) SPGR MRI image of the multi-modality spectroscopy phantom, (b) PET image of the phantom and (c) aligned phantom image.

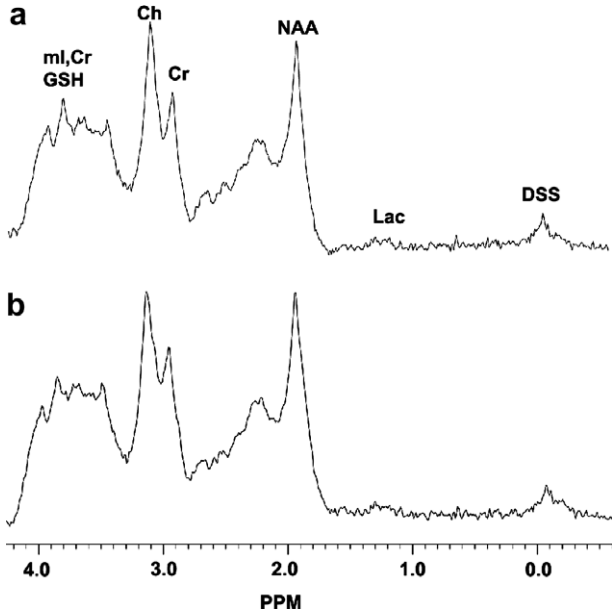

Fig. 3. PRESS localized 1D spectra acquired from the multi-modality spectroscopy brain phantom. The plot shown in (a) was acquired with the PET scanner component in place; the plot shown in (b) was acquired without the PET scanner in the MRI scanner.

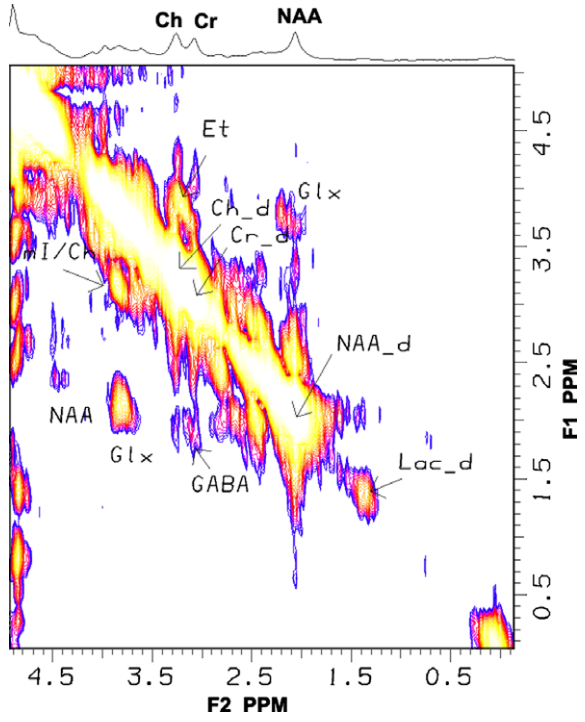

Fig. 4. Localized-correlated spectroscopy (L-COSY) spectrum acquired from the multi-modality sphere with the PET scanner in the MRI scanner. The spectrum shows the diagonal and cross peaks from the various chemical components of the metabolite solution.

respectively. There were no statistically significant differences ($p < 0.05$ for a two-tailed t-test) in the SNRs measured for the FSE and SPGR images with and without the PET imager in the MRI scanner. Fig. 3 shows 1D spectra of the PET–MRS brain phantom containing 17 metabolites as discussed in the earlier section. The top trace (a) shows the spectrum obtained with the PET imager in the magnet bore, the bottom trace and (b) shows the spectrum obtained without the PET imager in the magnet. The NAA/Cr metabolite ratios measured from the 1D spectra with the PET scanner in place and without the PET imager in the MRI scanner were 1.58 and 1.52, respectively (the actual ratio present in the phantom is 1.4). Fig. 4 shows the 2D L-COSY spectrum obtained from the PET-MRS phantom using the same VOI as used to acquire the 1D. The 2D spectrum shows well-resolved diagonal and off-diagonal resonances from several overlapping metabolites. The NAA/Cr ratios measured from the 2D L-COSY spectra with the PET imager in place and without the PET imager in the magnet bore were 1.32 and 1.28, respectively (the actual ratio in the phantom is 1.4). Finally, the line width of the water signal remained unchanged at 25.1 ± 1 Hz when the PET imager was placed in the MRI scanner.

4. Discussion

By combining the functional imaging capabilities of PET and MR, it may be possible to create novel methods that could benefit research and clinical procedures. The results shown in Fig. 2 demonstrate that our prototype MRI–PET scanner insert is capable of simultaneously producing good PET and MRI images. It should be noted that the angular under-sampling and small detector separation necessitated by the small diameter of the MRI head coil are non-optimal for producing PET images. Specifically, the limited-angle tomographic data available caused blurring of signal from the hot sphere to surrounding areas. We are planning to address these limitations in our second-generation imager by construction of a complete ring PET scanner. Nevertheless, the sphere is clearly visible in the PET and MRI images, validating our basic approach to creating a combined MRI–PET system. Significantly, the presence of the PET imaging insert inside the MRI scanner resulted in no detectable degradation of SNR measured from the SPGR and FSE image sets. This result is in contrast to the findings of the Tübingen group that reported an up to 20% reduction in SNR due to the shielding required for their APD-based PET imager [4]. By removing the photodetectors from the imaging volume of the MRI scanner, our system does not have any conductor that can degrade magnetic field homogeneity, reducing SNR (as did the Tübingen group's device). The downside to this method is loss of energy resolution due to loss of scintillator light in the light guides. We are currently working on methods to address the phenomenon without impacting MRI SNR. It should be noted that scaling a light guide-based system up to a size suitable for small animals (axial FOV = ~5 cm and transaxial FOV = ~12 cm) is feasible; a system much larger than this size (suitable for humans, for example) would be bulky and not optimal for clinical use.

The capabilities of our prototype system are further illustrated by the good quality 1D and 2D L-COSY spectra

shown in Figs. 3 and 4. For example, in Fig. 3 note that there are no discernable differences in the complex 1D spectra of the brain phantom obtained with and without the PET imager in the MRI scanner. Our estimates of the metabolite ratio NAA/Cr were in reasonable agreement with the actual concentration of the metabolites. Furthermore, there were negligible differences between these metabolite ratios measured with and without the PET imager inside MRI scanner.

Compared to the 1D spectrum, the 2D L-COSY spectrum shown in Fig. 4 demonstrates the separation of overlapping metabolites possible through spectral cross peaks arising from coherence transfer between various scalar-coupled resonances. Specifically, note the clarity of the GABA cross peak [$F_1 = 3.00$ and $F_2 = 1.9$ ppm], which is a particularly challenging metabolite to identify with conventional 1D localized MRS techniques. As with the 1D spectra, there were no qualitative differences between the 2D COSY spectra obtained with and without the PET scanner inside the MRI scanner. Finally, the COSY-spectra-derived estimates of the NAA/Cr ratio showed negligible difference with and without the PET scanner in the MRI system. Again demonstrating that the design of our PET system has minimal or no effect on MRS measurements.

5. Conclusions

In conclusion, the complementary information acquired by simultaneously acquiring PET and MRS data may have an important impact on the *in vivo* investigation of a number of complex physiological processes. In this study, we have demonstrated that a system design utilizing fiber optic light guides to couple the scintillator and light detection units (PMTs) can be used to obtain contemporaneous MRS spectra (or MRI images) and PET images without any indication of loss in image or data quality. These results may pave the way for creation of more complex imagers that will permit continued study of this new area of multi-modality, complementary imaging. Future work includes the construction of a full detector ring suitable for small animal imaging integrated with a custom MRI coil.

Acknowledgments

This work was supported by the National Cancer Institute (Grant No. R01 CA094196) and by the Office of Science of the U.S. Department of Energy. Jefferson Science Associates, LLC operates the Thomas Jefferson National Accelerator Facility for the U.S. Department of Energy under U.S. DOE Contract No. DE-AC05-06OR23177.

References

[1] B. Pichler, E. Lorenz, R. Mirzoyan, Performance test of a LSO-APD PET module in a 9.4 Tesla magnet, IEEE Nucl. Sci. Symp. Conf. Rec. 2 (1997) 1237–1239.

[2] A. Saoudi, R. Lecomte, Novel APD-based detector module for multi-modality PET/SPECT/CT scanners, IEEE Trans. Nucl. Sci. 46 (1999) 479–484.

[3] R. Grazioso, N. Zhang, J. Corbeil, M. Shmand, R. Ladebeck, M. Vester, G. Schnur, W. R, H. Fischer, APD-based PET detector for simultaneous PET/MR imaging, Mol. Imaging 4 (2005) 391 (abstract).

[4] B.J. Pichler, M.S. Judenhofer, C. Citrana, J.H. Walton, M. Kneiling, R.D. Nutt, S.B. Siegel, C.D. Claussen, S.R. Cherry, Performance test of an lso-apd detector in a 7-T MRI scanner for simultaneous PET/MRI, J. Nucl. Med. 4 (2006) 639–647.

[5] C. Catana, Y. Wu, M.S. Judenhofer, J. Qi, B.J. Pichler, S.R. Cherry, Simultaneous acquisition of multislice PET and MR images: initial results with a MR-compatible PET scanner, J. Nucl. Med. 47 (2006) 1968–1976.

[6] N.L. Christensen, B.E. Hammer, B.G. Heil, K. Fetterly, Positron emission tomography within a magnetic field using photomultiplier tubes and lightguides, Phys. Med. Biol. 40 (1995) 691–697.

[7] R. Slates, S.R. Cherry, A. Boutenfouchet, Y. Shao, M. Dahlborn, K. Farahani, Design of a small animal MR-compatible PET scanner, IEEE Trans. Nucl. Sci. 46 (1999) 565–570.

[8] G.M. Haak, N.L. Christensen, B.E. Hammer, Coupling scintillation light into optical fibre for use in a combined PET–MRI scanner, Nucl. Instr. Meth. A 399 (1997) 455–462.

[9] P.B. Garlick, P.K. Marsden, A.C. Cave, H.G. Parkes, R. Slates, Y. Shao, R.W. Silverman, S.R. Cherry, PET and NMR dual acquisition (PANDA): application to isolated, perfused rat hearts, NMR Biomed. 10 (1997) 138–142.

[10] M. Buchanan, P.K. Marsden, C.H. Mielke, P.B. Garlick, A system to obtain radiotracer uptake data simultaneously with NMR spectra in a high field magnet, IEEE Trans. Nucl. Sci. 43 (1996) 2044–2048.

[11] M.F. Smith, R.R. Raylman, S. Majewski, A.G. Weisenerger, Positron emission mammography with tomographic acquisitions using dual planar detectors: initial evaluations, Phys. Med. Biol. 49 (2004) 2437–2452.

[12] R.R. Raylman, S. Majewski, S.K. Lemieux, S.S. Velan, B. Kross, V. Popov, M.F. Smith, A.G. Weisenberger, C. Zorn, G.D. Marano, Simultaneous MRI and PET imaging of a rat brain, Phys. Med. Biol. 51 (2006) 6371–6379.

[13] V. Govindaraju, K. Young, A.A. Maudsley, Proton NMR chemical shifts and coupling constants for brain metabolites, NMR Biomed. 13 (2000) 129–153.

[14] P.A. Bottomley, Spatial localization in NMR spectroscopy in vivo, Ann. N.Y. Acad. Sci. 508 (1987) 333–348.

[15] J. Pauly, P. LeRoux, D. Nishimura, A. Macovski, Parameter relations for the Shinnar–LeRoux selective excitation pulse design algorithm, IEEE Trans. Med. Imag. 10 (1991) 53–65.

[16] U. Seeger, U. Klose, D. Seitz, T. Nagele, O. Lutz, W. Grodd, Proton spectroscopy of human brain with very short echo time using high gradient amplitudes, Magn. Reson. Imag. 16 (1998) 55–62.

[17] S.W. Provencher, Estimation of metabolite concentrations from localized in vivo proton NMR spectra, Mag. Reson. Med. 30 (1993) 672–679.

[18] M.A. Thomas, K. Yue, N. Binesh, P. Davanzo, A. Kumar, B. Siegel, M. Frye, J. Curran, R. Lufkin, P. Martin, B. Guze, Localized two-dimensional shift correlated MR spectroscopy of human brain, Magn. Reson. Med. 46 (2001) 58–67.

[19] S.S. Velan, C. Durst, S.K. Lemieux, R.R. Raylman, R. Sridhar, R.G. Spencer, G.R. Hobbs, M.A. Thomas, Investigation of muscle lipid metabolism by localized one- and two-dimensional MRS techniques using a clinical 3T MRI/MRS scanner, J. Magn. Reson. Imag. 25 (2007) 192–199.

[20] S.S. Velan, S. Ramamurthy, S.K. Lemieux, R.R. Raylman, M.A. Thomas, Unravelling Glutathione and other low concentration cerebral metabolites using 2D correlated spectroscopy on a 3T MRI scanner, Proc. Int. Soc. Magn. Reson. Med. 13 (2005) 2495.